A. A. ElFouly / ICEHM2000, Cairo University, Egypt, September, 2000, page 599- 611

Spatial relations of the fracture intersections, hydrothermal alterations and the aeroradiometric measurements for selected areas at the North Eastern Desert, Egypt and their health risk considerations

Adel ElFouly
Cairo University, Geology Department, Giza, Egypt.
AdelElFouly@OREX.ORG

Abstract: This study investigates the relation among secondary fractures associated with main fault systems and the hydrothermal alterations, iron enrichments, lithologic variations and the intensity of the aeroradiometric measurements in the study areas. The surface geology of the selected areas is dominated by basement exposures flanked by younger sedinentary formations ranging from Mesozoic to Tertiary in age. Granites-granodiorites, metavolcanics and metasediments represent the major rock types of the basement. This study revealed the consistancy and inconsistancy of the linear patterns inferred from the density of lineament intersections (DLI) that belong to the caculated 1st principle component, the enhanced hydrothermal altration in TM bands 5/7 and the enhanced iron enrihment inTM bands 3/1 with the linear patterns observed in the aeroradiometric measurements in these areas. The direct relation of the DLI linear patterns to major structural elements in the selected areas are discussed. This study, is shading the light on the possible health hazard due to the high values of aeroradiometric measurements and the relatively high wind speed in the area.

Introduction:

The purposes of this study are 1) to determine the interpolated density of lineament intersection pattern extracted from TM Landstat-5 images for selected areas in the region (Fig. 1) and to check their consistency with the aeroradiometric measurments. 2) to distinguish any possible differences in the shear distribution pattern and their relation with aeroradiometric measurements variations. 3) to distinguish any shear pattern that is directly affiliated major structural elements in the selected areas. 4) to study the possiblility of health hazards sources due to high values of radiometric measurements. Aeroradiometric maps of the area (Acro Service, 1984) were studied for the different radiometric patterns.

The earliest use of Satellite remote sensing for metals was for uranium for two reasons, one economic and the other technical. First, the market for uranium was strong in the early 1970s when LANDSAT 1 was lauched, and the major oil companies became active in its exploration about that time. Second, ferric oxides, which are associated with the geochemical cells that are important for uranium concentration could be mapped with data from the MSS scanner and TM of the LANDSAT series.

The LANDSAT spectral ratio data were in image form, which made it easier for geologists to separate features of possible for them to visually verify the ferric oxides in the field. The collapse in uranium commodily prices within the next few years kept all of those prospect areas from becoming economic, but a fast, inexpensive, new exploration tool for uranium was born.

Geomorphologic and Geologic Setting:

The area studied located in the northeastern part of Egypt. It has maximum limits of lat.27°15'and lat.28°15'N and long.32°30'and long.33°45'E.The studied area at the North Eastern part of the Eastern Desert region is geomorphologically divisible into three main units, namely: a coastal plain flanking the Gulf of Suez, a western mountainous chain and, linear inliers of basement exposures that parallel the general trend of the Gulf of Suez (Fig.1). The coastal plain is a narrow strip of low land between the Gulf of Suez and the western mountainous terrain. It is covered by Middle Tertiary to Quaternary sediments, and extensive gravel and sand deposits form a gently seaward sloping terrace incised by shallow wadis

which drain the mountainous chain west of the plain. Indurated Tertiary deposits rise as inliers through the terrace in small low-lying hills and hummocks. The plain is interrupted by the basement inliers of Esh Mellaha, Gebel Zeit Overlooking it from the east.

The western mountainous chain represents a rugged and deeply dissected exposure of the Egyptian basement complex, a part of the Arabo-Nubian massif. Crest elevations up to 1100 meters are not uncommon although height is about 700 m. Most of the main wadis draining this area originate in these mountains which form the primary watershed separating the Gulf of Suez-Red sea drainage basin from that of the Nile farther west. The eastern edge of this basement is believed to represent a retreating fault scarp with the actual fault (or faults) being concealed beneath the younger sedimentary cover.

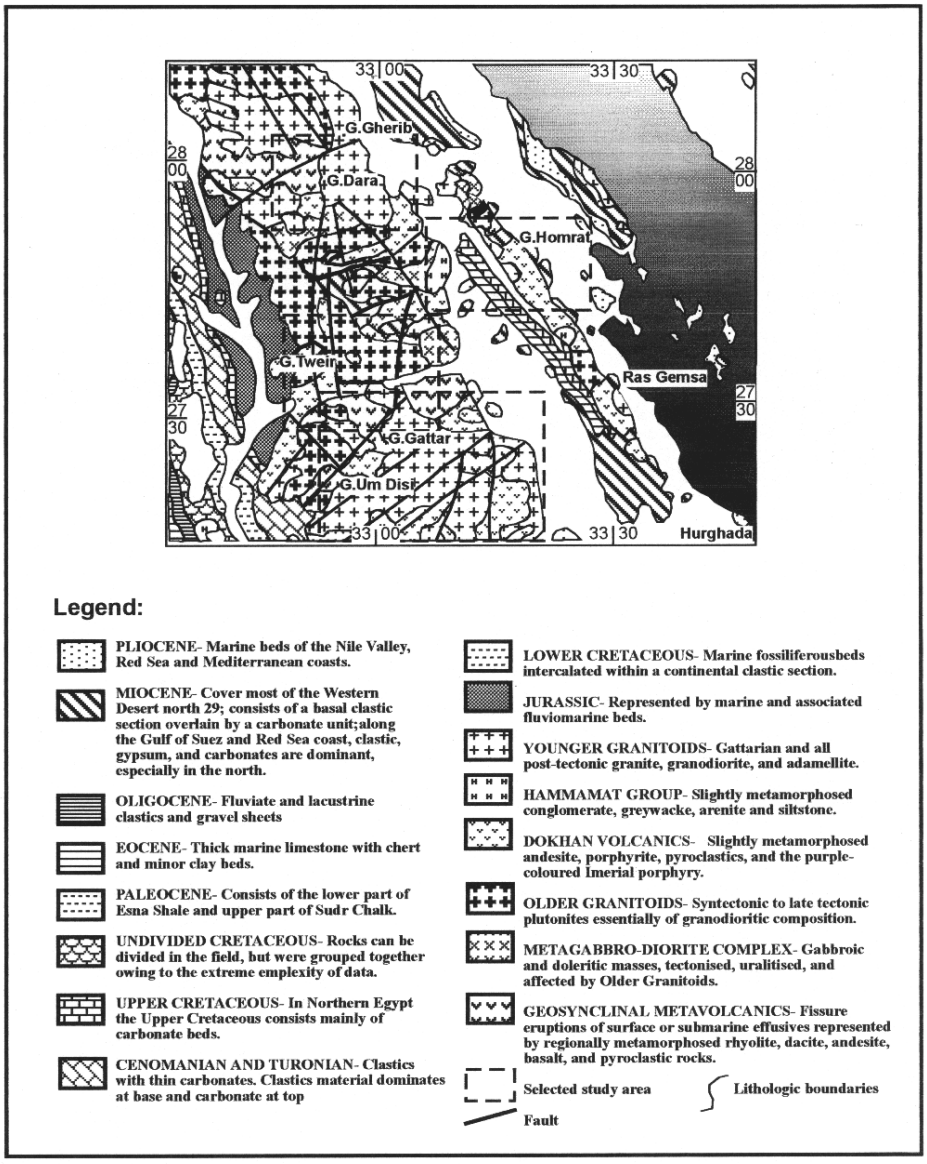

Fig.1 Geologic map of the area northeast the Eastern Desert, Egypt, reproduced from the Geological map of Sinai, Sheet NO.1, 1994. Geologic survey of Egypt, Arab Republic of Egypt.

The linear ranges of Esh Mellaha, Gebel Zeit, and Gebel Araba-Gebel Durba generally parallel the Gulf of Suez and are actually faulted of lower elevation than the western mountain chain (average 400 m). Basement rocks from the bulk composition of these ranges flanked by younger sedimentary rocks producing a much more subdued relief.

Figure 1, is a reproduction of part of the recent geological map of Egypt (Geol. Surv. Egypt, 1994) covering the selected areas under study. The area distribution of the different rock units and their chronological order are elucidated. Batholithic granities and granodiorites cover more than 60% of the surface area of the basement exposure. In the Egyptian basement. Cretacoeus and Eocene formations dominate the area occupied by indurated sedimentary cover.

Procedure of study:

The Procedure of study of the current work is designed to examine the consistency of the interpolated density of lineament intersection (DLI) with the aeroradiometric measurments of the study areas and to demonstrate the possible differences in the lineation pattern with related radiometric variations.The density of lineament intersection (DLI) (ElFouly, 1992) method was adapted in the present study. The current study procedure will be discussed breifly in the following four stages.

First, the spectral bands 1,3,4,5,and 7 are selected from the seven the landsat TM Landstat-5 scene to be calculated for the study area. As El Amin (1975) concluded that the uranium bearing hydrothermal solutions rose along major fundamental fractures trending NE-SW and concentrated their uranium mineralization in the N-S and NNE-SSW trending joints. He added that, the association of hematitization and other alteration features with the high δ radioactivity suggests its hydrothermal origin. The ratioing of band 5 over band 7 is recommended for the production of hydrotermal alteration enhacement layer. Ferric oxides are important for uranium concentration. The ratioing of band 3 over band 1 are preferred for the production iron enrichment enhanced layer.

Second, the application of the lineament intersection operator (ElFouly, 1992) on the hydrothermal alteration enhanced and iron enrichment enhanced layer of stage I. This procedure is a very powerful way to delineate the intersected lineaments that only related to hydrothermal alteration or iron enrichments in separate layers. The output of this procedure will be layers with only dots for each of the above mentioned ratios.

Third, each of the produced layers of lineament intersection in the stage II is counted per kilometer square and interpolated to produce three Density of lineament intersection maps.

Fourth, the indentification of linearly oriented pattern related to arrangements of density of lineaments of intersection. This pattern will be delineated and compaired with the aeroradiometric measurements and to known structures in the selected areas.

Spectral Bands selection, ratioing and Principle Components analysis

The application of band ratioing

Band rationing is used in this study to enhance the spectral reflection related to hydrothermal alteration and iron enrichments. The simple act of dividing numerical values in one band by those in another for each pixel to produce ratioing images is the most widely used technique for discriminating lithologies and other surface cover types in a scene. The method produces images in which radiance variation that is proportionally constant from band to band is suppressed and the more interesting radiance variance attributable to spectral reflectance of geological materials is enhanced.

Band selection for ratio image depends on the spectral properties of the surface material of interest and its abundance relative to other surface cover types. Usually, numerator band is chosen in which the material is highly reflective and a band covering an absorption feature for that material is chosen as the denominator.correlation analysis of TM data by Crippen (1988) showed that for arid areas, a combination that includes one from the long-wavelength bands (TM 5, 7) and one ratio with bands from each group produces the best discrimination of geological materials. His analysis and experience of numerous investigators have shown that TM 3/1 best discriminates ferric oxides, and TM 5/7 discriminate materials containing

hydroxyl-bearing minerals and carbonates with absorption features in the region 2.2 to 2.3 μm (Brickey, 1986; Hutsinpiller, 1988; Kowalczyk and Logan, 1989; Bennett, 1993; Sabins and Miller, 1994).

Alunite and hydrothermal clay minerals have distinctive absorption features (reflectance minima) at wavelength within the bandpass to TM band 7. These minerals have higher reflectance values within TM band 5. The TM ratio 5/7 is effective for recognizing clays and alunite. The reflectance of unaltered rocks in band 7 is similar to that in band 5. Therefore the bands 5/7 ratio for unaltered rocks is unity (1.00). Altered rocks, however, have lower reflectance in band7 because of absorption caused by the minerals. Therefore the 5/7 ratio for altered rocks is much greater than unity.

Iron minerals are the second indicators of hydrothermally altered rocks. Spectra of the iron minerals that have low blue reflectance (TM band 1) and high red reflectance (TM band 3). Iron-stained hydrothermally altered rocks threrefore have high values in a TM band 3/1 ratio image.

The application of Principle Components analysis:

Most of the variation of radiant spectral Flux measured by a sensor depends on slope aspect relative to solar illumination and albedo effects at the surface. Very little of this variation arises from spectral reflectance features of surface naterials. Principlal component analysis (PCA) is a powerful means of supperssing irradiance effects that dominate all bands so that geologically intersting spectral reflectance features of surface materials can be examined. PCA is also useful reducing the dimensionality of multispectral data and the high degree of band-to-band correlation that is inherent in such data sets.

A principal component (PC) transformation entails data rotation and translation to a new set of statistically independent orthogonal axes which are the principal components (eigenvalues of the covariance matrix) of the data set. The origin of the new coordinate system is the mean of the original data set. The number of PCs is the same as the number of spectral bands used in the transformation. For each PC, new numerical values are assigned to each pixel according to its new coordinates and may have no relationship to values in the original data. PC 1 is usually dominated by illumination effects arising from differences in slope aspect relative to the sun and provides a good noise-free representation of topography. Spectral reflectance features of surface materials and noise appear in higher-numbered PCs. Because PCA is a statistical procedure, the information in each PC is scene dependent. PCA has been used extensively to extract information related to host rocks, mineralization, and alteration from TM imagery (e.g., Mouat et al., 1986; Amos and Greenbaum, 1987; Eriksen and Cowan, 1989; Frei and Jutz, 1989; Rodrigeuz and Glass, 1991; Bennett, 1993).

Lineaments Intersection extraction

A highly non-linear logic operators are used to extract lineaments and their intersections from Landsat-5 images have been introduced by El-Fouly, 1992 and El-Fouly et.al., 1992. These operators calculate the gradient along 2 axial and 2 diagonal orientations among adjacent pixels. This step is followed by a series of table lookups and logical binary decisions to determine the presence or absence of the feature of the lineaments or their. The logic OR will extract the lineaments and the logic AND will detect their intersection.

The production of the interpolated Density of lineaments intersection (DLI) Layers

The densities of lineament intersection analysis and its application can be described using the faulting example (ElFouly 2000) produced in the experiments carried out by Wilcox, Harding and Seely (1973) that exemplifies the geometry and kinematics of Riedel shearing, which is characteristic of, but not limited to, strike-slip faulting.

The whole concept of Riedel shearing gives us a better sense of why strike-slip fault zones have a braided appearance and how the points of intersections will help us delineate the main line of faulting. By calculating the density of the intersected minor faults, and interpolating the output, the density of lineaments intersections map will be produced Any the elongated pattern in this map can point a main line of faulting in the area.

The density of lineaments intersection is the number of intersected lineaments per kilometer square. The interpolated DLI will help delineate main shear zones. The DLI related to the enhanced hydrothermaly altered and iron enriched fractures in the area can be observed in figure (2c,2e,3c,3e,4c,4e,5cand 5e). Since the DLI related to the calculated first principle component of the study area which have the largest percentage of the total scene variance, represent the intensity and location of the possible conduits related to most lithologic unit in the area (fig.2d,3d,4d,and 5d).

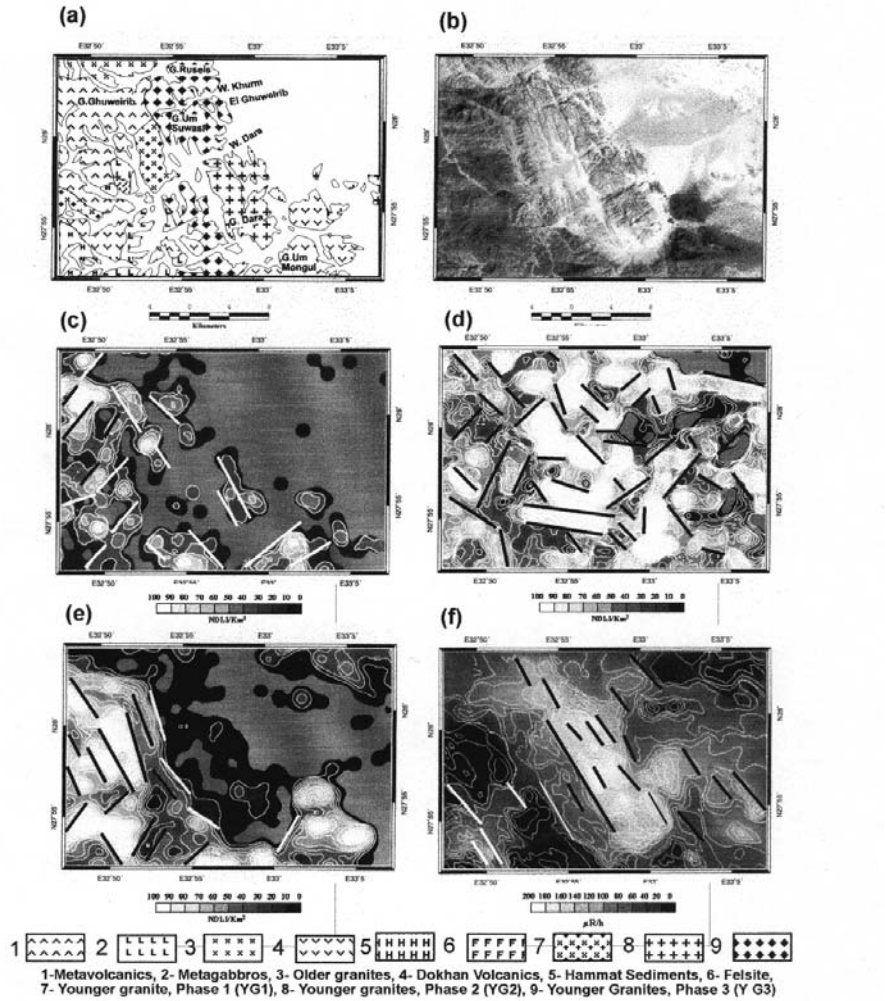

Fig. 2: (a) Photogeologic Geologic map around G.Dara and G.Ghuweirib,(b) Corresponding monochromatic image of the first principal component of the TM landsat-5 image. (c) Corresponding normalized density of lineaments intersection of TM landstat-5 band#5/ band#7 showing the linear patterns of the intersected lineaments associated with hydrothermal alterations. (d) Corresponding normalized density of lineaments intersection of the first principle component of the band#1,2,3,4,5 and 7 of the TM landsat-5 satelite image. (c) Corresponding normalized density of lineaments intersection of TM landstat-5 band#3 over band#1 showing the patterns of intersected lineaments associated with iron enrichments. (f) Corresponding aeroradiometric contour and intensity map of the same localities.

Delineation and comparison of the linear patterns

The following few paragraphs are dealing with the indentification of linearly oriented patterns related to arrangements of the density of lineaments of intersection for the hydrothermal alteration, iron enrichments associated with alteration and the calculated 1st principle components of six TM bands of the selected areas. The various linear patterns will be induced and compaired with patterns with the aeroradiometric measurements to understand the characteristic relations of the radiometric measurements and the main stuctures in these areas.

Linear patterns distribution in the area around G. Dara and G. Ghuweirib areas

In figure 2c, the induced linear shear related density of lineaments intersection of TM Landstat-5 band5/7 show patterns of the intersected lineaments associated with hydrothermal

alterations. The NE-SW direction is dominating the western part of this area at G. Ghuweirib and at the south eastern part at G. Um Mongul. The NW-SE direction can be observed at the eastern part of G. Ghuweirib. The western part of G. Um Suwasi and the western part of G. Dara.

In figure 2d, the induced linear shear related to density of lineaments intersection of the calculated first principle component of band 1,2,3,4,5 and 7 of the TM landsate.The NW-SE direction is observed at G.Ghuwerib, G. Um Suwasi and partly at G. Dara. The NE-SW direction is defined at eastern part of the area and at G. Dara. The NE-SW direction is defined at the eastern part of this area and at G. Dara. The NWW-SEE direction is observed west of G.Dara.

In figure 2e, the linear shear related to density of lineaments intersection of TM Landstat-5 band 3 over band 1 showing the patterns of intersected lineaments associated with iron enrichments. Iron rich related shear directions can not be detected in the western part of this area. The NW-SE direction is generally observed south of G. Ghuweirib. We can not record anything at G. Dara, G. Um Suwasi. The NE-SW direction dominating the southern part of this area.

In figure 2f, an aeroradiometric intensity map of the same localities The NW-SE direction is the only direction recorded in the area. This direction is concentrated at G. Dara, G. Um Suwasi and the soth western part of the area.

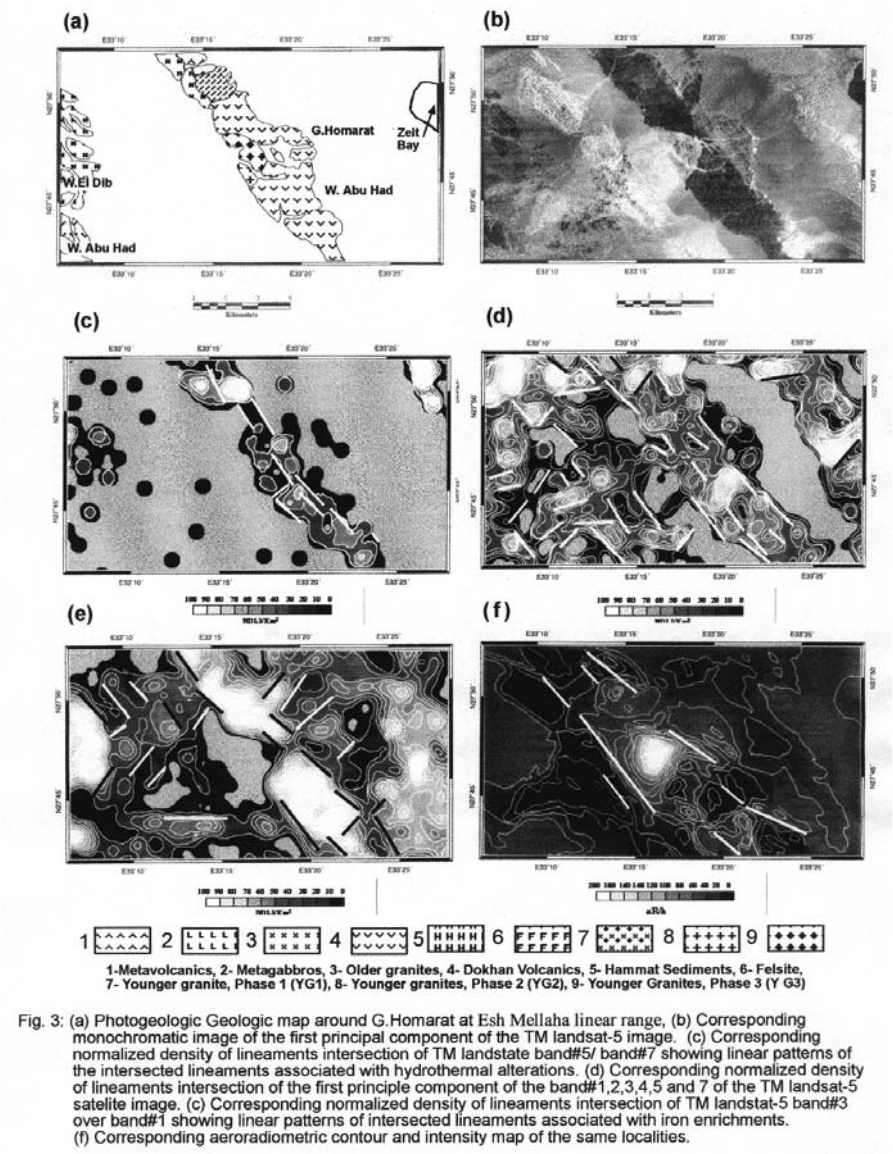

Fig. 3: (a) Photogeologic Geologic map around G.Homarat at Esh Mellaha linear range, (b) Corresponding monochromatic image of the first principal component of the TM landsat-5 image. (c) Corresponding normalized density of lineaments intersection of TM landstate band#5/ band#7 showing linear patterns of the intersected lineaments associated with hydrothermal alterations. (d) Corresponding normalized density of lineaments intersection of the first principle component of the band#1,2,3,4,5 and 7 of the TM landsat-5 satelite image. (c) Corresponding normalized density of lineaments intersection of TM landstat-5 band#3 over band#1 showing linear patterns of intersected lineaments associated with iron enrichments. (f) Corresponding aeroradiometric contour and intensity map of the same localities.

Linear patterns distribution in the area around G. Homarat at Esh Mellaha range

In figure 3c, the induced linear shear related to density of lineaments intersection of TM Landstat-5 band5/7 show the patterns of the intersected lineaments associated with hydrothermal alterations.The NW-SE direction is restricted along the Ash Melaha range. The less dominant NE-SW direction is restricted only north of W. Abu Had.

In figure 3d, shears related to density of lineaments intersection of the first principle component of the band1,2,3,4,5 and 7 of the TM landsate. The NW-SE and the NE-SW dirctions are recorded. The NW-SE are the dominant and located all over Ash Malaha range.

In figure 3e, shears related to density of lineaments intersection of TM Landstat-5 band 3 over band 1 showing the patterns of intersected lineaments associated with iron enrichments. The NW-SE direction is dominating the basement rocks of Ash Melaha range and the NE-SW is found in the surrounding recent deposits.

In figure 3f, an aeroradiometric contoured intensity map of the same localities The NW-WE direction is bounding the Ash Melaha range along it eastern and western borders.

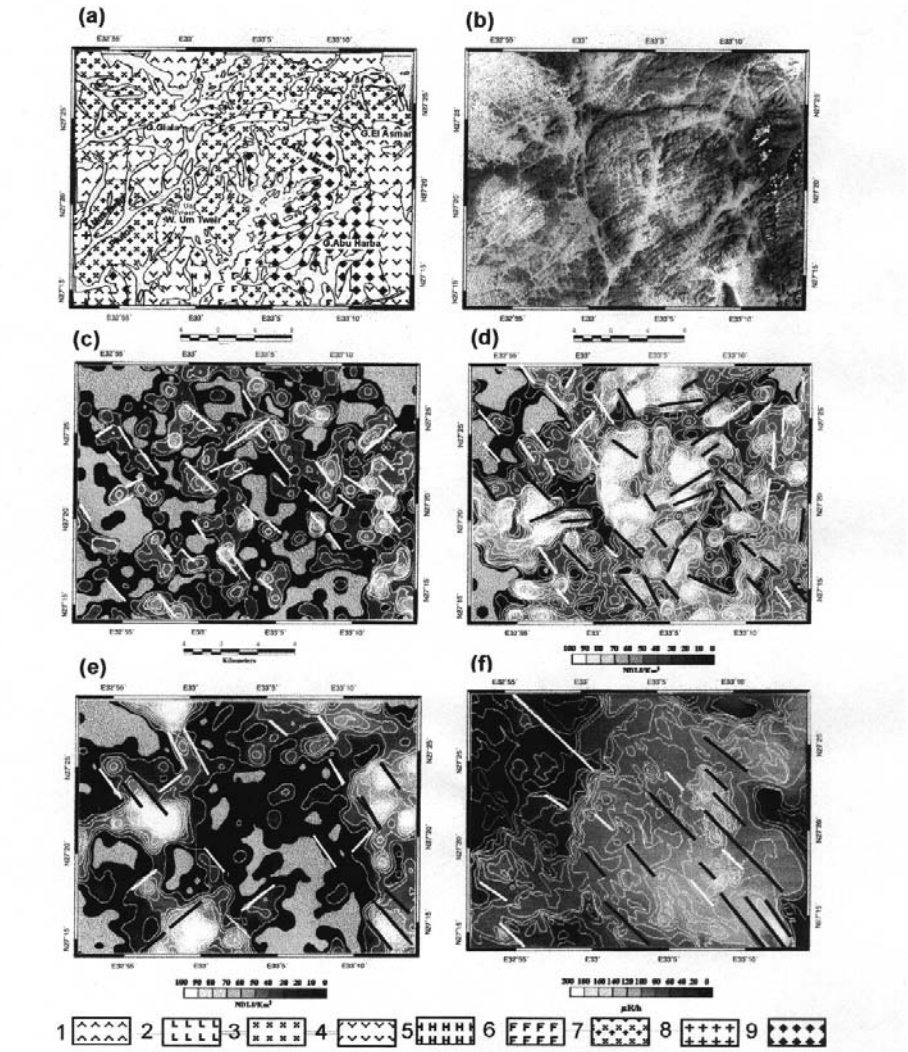

Fig. 4: (a) Photogeologic Geologic map around G.Um Tweir and G. Abu Marwa, (b) Corresponding monochromatic image of the first principal component of the TM landsat-5 image. (c) Corresponding normalized density of lineaments intersection of TM landstate band#5/ band#7 showing linear patterns of the intersected lineaments associated with hydrothermal alterations. (d) Corresponding normalized density of lineaments intersection of the first principle component of the band#1,2,3,4,5 and 7 of the TM landsat-5 satelite image. (c) Corresponding normalized density of lineaments intersection of TM landstat-5 band#3 over band#1 showing linear patterns of intersected lineaments associated with iron enrichments. (f) Corresponding aeroradiometric contour and intensity map of the same localities.

Linear patterns distribution in the area around G. UmTweir and G. Abu Marwa

In figure 4c, shears related to density of lineaments intersection of TM Landstat-5 band 5/ band 7 shows the patterns of the intersected lineaments associated with hydrothermal

alterations. The NW-SE direction is the dominant direction in this area especially north of G. Abu Harba, south of G. El Asmar, at G. Abu Marwa and south east G. Um Tweir. The NE-SW direction can be observed north west G. Um Tweir, North west G. Abu Marwa and G. El Asmar.

In figure 4d, shears related to density of lineaments intersection of the first principle component of the band 1,2,3,4,5 and 7 of the TM landsate. The NW-SE direction is dominating the western part of G. Giala and Um Tweir. This direction can be observed clearly at G. Abu Harba in the South eastern corner of this area. The NE-SW direction is observed at G. Abu Marwa and the NNE-SSW direction is cutting W. Um Tweir in South western part and observed parallel to the felsites of north G. Abu Marwa in the North eastern part of the area.

In figure 4e, the induced linear shear related to density of lineaments intersection of TM Landstat-5 band#3 over band 1 showing the patterns of intersected lineaments associated with iron enrichments.The NW-SE is detected arround G.Giala in the North western part at G.El Asmar in the north eastern part and south easter G. Abu Harba in the south eastern part. The NE-SW is detected in the south western part south of G. Um Tweir and at G. Giala.

In figure 4f, an aeroradiometric contoured intensity map of the same localities. The Nw-SE are the only direction in the area and is concentrated at G. Abou Harba and G. Abu Marwa in the eastern and south eastern parts of the area.

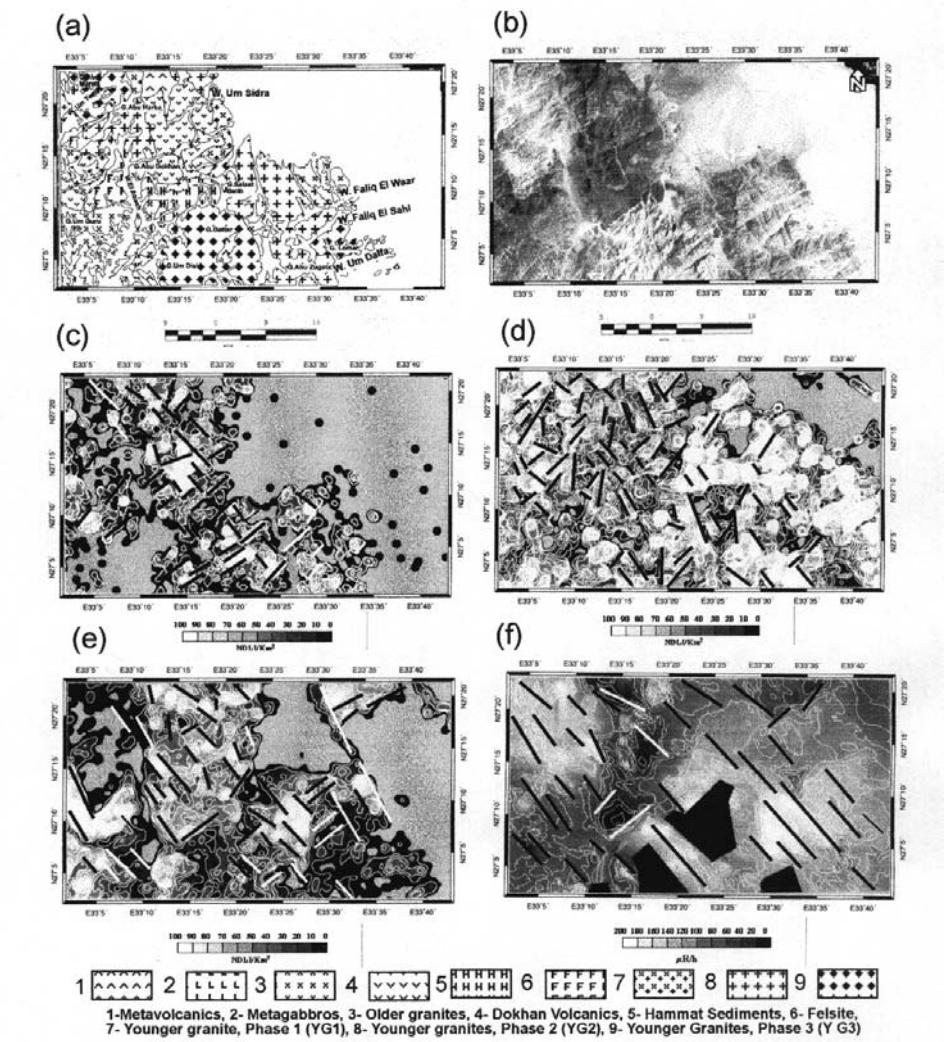

Fig. 5: (a) Photogeologic Geologic map around G.Salaat Belih, G. Gattar and G. Abu Harba, (b) Corresponding monochromatic image of the first principal component of the TM landsat-5 image. (c) Corresponding normalized density of lineaments intersection of TM landstat-5 band#5/ band#7 showing linear patterns of the intersected lineaments associated with hydrothermal alterations. (d) Corresponding normalized density of lineaments intersection of the first principle component of the band#1,2,3,4,5 and 7 of the TM landsat-5 satelite image. (c) Corresponding normalized density of lineaments intersection of TM landstat-5 band#3 over band#1 showing linear patterns of intersected lineaments associated with iron enrichments. (f) Corresponding aeroradiometric contour and intensity map of the same localities.

Linear patterns distributions in the area around G.Salaat Belih, G. Gattar and G. Abu Harba areas:

In figure 5c, the induced linear shear related to density of lineaments intersection of TM landstat-5 band 5/band 7 showing the patterns of the intersected lineaments associated with hydrothermal alterations. Two main trends can be observed along the NW-SE and NE-SW directions. The NW-SE is well defined at G.Abu Harba, East of G. Abu Dokhan. The Northern part of G. Gattar and G. Abu Zugata. The NE-SW direction can be defined at G. Um Guru, G. Um Disi, G. Abu Zugata, G. Lomar and the North eastern part of G. Abu Harba.

In figure 5d, the induced linear shear related to density of lineaments intersection of the first principle component of the band 1,2,3,4,5 and 7 of the TM landsate The NE-SW directions are presented along W. Um Tweir, in the north western part of the area. The same direction can be recorded in the south eastern part of G. Gattar, north G. Um Guru and north G. Salaat Belih. The NW-SE direction can be seen east of G. Abu Harba, north G. Abu Dokhan and north G. Gattar, at G. Salaat Belih and G. Abu Zugata.

In figure 5e, a shear related to density of lineaments intersection of TM Landstat-5 band 3 over band 1 show the patterns of intersected lineaments associated with iron enrichments.The NW-SE direction is the main trend in this area. This trend can be observed at G. Abu Harba, G. Abu Dokhan, North and South G. Um Guru, east G. Gattar, north G. Abu Zugata and east G. Salaat Belih. The NE-SW direction is abserved in the central, eastern and south eastern parts of the area.

In figure 5f, an aeroradiometric intensity map of the same localities The NW-SE direction is the main trend in this area. The NE-SW and the NW-SE trends are objeserved at the anomaly shown north of G. Gattar. In the North eastern part the NW-SE directions is observed at the high radiometric values of G. Abu Marwa in the north western corner of the area.

Radioactivity Trend analysis:

A study of aeroradiometric maps of the selected areas reveal that the younger granitic rocks display higher radioactivity levels than the other basement rock units.The radioactivity trend of the study area shows a dominant trend in the N 45° W direction (Figs. 2f, 3f, 4f, and 5f) which is almost parrallel to the NW- trending fracture system of the study area. N 45° E represent the next subdominant radioactive trend which is transverse to the Red sea. The NW elongation of the radioactivity in the direction and its predominance over the other trend is striking feature in the area. This can be explained considering the general elongation of the basement outcrops especially the Younger Granite plutons in a NW-trending along the younger folding axes in the Eastern Desert (Abdel Meguid, 1986) and the later NW major faults governing the outcrops in the area. Most low and moderate radioactive contours elongate parallel to this trend. The steep gradients observed at the contact between the rock groups are generally elongated in a NW direction (Figs. 2f, 3f, 4f, and 5f) . This reflects a lithologic expression of this radioactivity trends. On the other hand, most of the high values are elongated NW relfecting a structural control of the radioactivity along this trend. This may indicate a later rejuvenation of NW-trending fracture system and indicates probable lithological and structural control.

The NE Trend is of minor existence and cuts through the boudaries of the different Younger Granitic plutons.It also cuts through some of the NW-trending higher contour levels as in G. Loman (fig. 6), where the NW-trending contours of 160 μR/h are laterally displayed along NE direction at the north western part of G. Loman.

The N-S to NNW trends are well represented in the northern part of G.Gattar, G. Salaat Belih and G. Abu Harba (Fig. 6). They are represented by contours >160 μR/h within areas about 120 and 130 μR/h. In G. Abu Harba, the N-S and NNW radioactivity trends are related to the major macro-lineament structures. In G. Salaat Belih, they occur along the micro-

lineament structures. Some uranium occurrences were found associated with this trend in G. Gattar. In conclusion, the anomalously high levels radioactivity are controlled by the NW, NNW and N-S trends (Fig. 2f, 3f, 4f, 5f, and 6). The NE trend is considered to be of secondary importance, helping in the concentration of the highest anomalies along its intersection with the main NW, NNW and N-S trends.

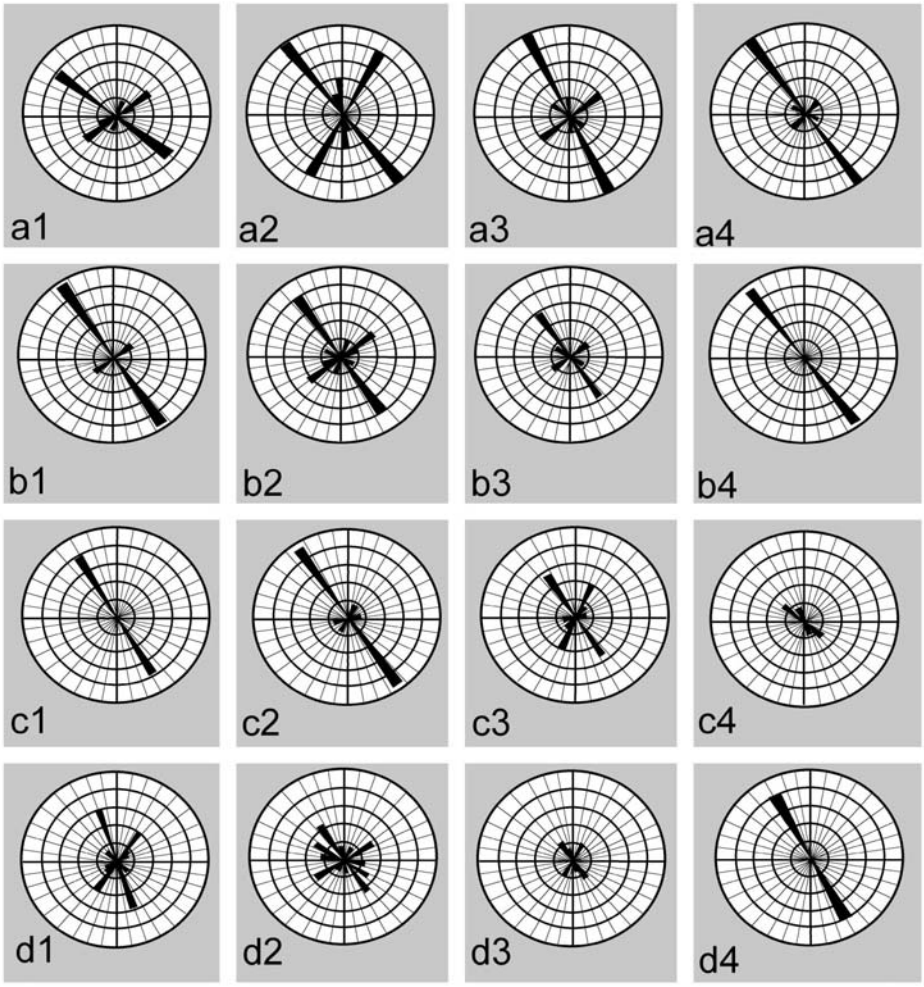

Fig. 6: (a1,a2,a3,&a4) Rose diagrams around G.Dara and G.Ghuweirib, (b1,b2,b3,&b4) around G.Homarat at Esh Mellaha linear range, (c1,c2,c3,&c4) around G.Um Tweir and G. Abu Marwa, and (d1,d2,d3,&d4) around G.Salaat Belih, G. Gattar and G. Abu Harba showing at (a1, b1,c1, &d1) trend directions of the linear patterns of the intersected lineaments associated with hydrothermal alterations extracted from the normalized density of lineaments intersection of TM landstat-5 band#5/ band#7 . (a2,b2, c2, & d2) showing trend directions of the linear patterns associated with the normalized density of lineaments intersection of the first principle component for band#1,2,3,4,5 and 7 of the TM landsat-5 satelite image. (a3,b3,c3,&d3) trend directions of the linear patterns associated with iron enrichments of the normalized density of lineaments intersection of TM landstat-5 band#3 over band#1. (a4,b4,c4,&d4) trend directions for aeroradiometric contour and intensity map of the above mentioned localities.

Radioactivity and Health risk

figure 7 depicts annual distribution of mean wind speeds obtained from the data. From the Figure, it can be shown that mean speed ranges from 2.0 to 7.5 $m.s^{-1}$. Areas of maximum speeds are located at Gulf of Suez, Port Said, Ras benass, and around Nasser Lake. The wind speeds are higher in summer than those in winter. This may due to the high contrast between sea surface temperature and that of land in summer season (El-Asrag et al., 2000).

In the study area the mean speed ranges from 4.5 to 7.5 $m.s^{-1}$. This speed is considered high and can generate large amounts of natural dust that can effect areas along the wind pass.

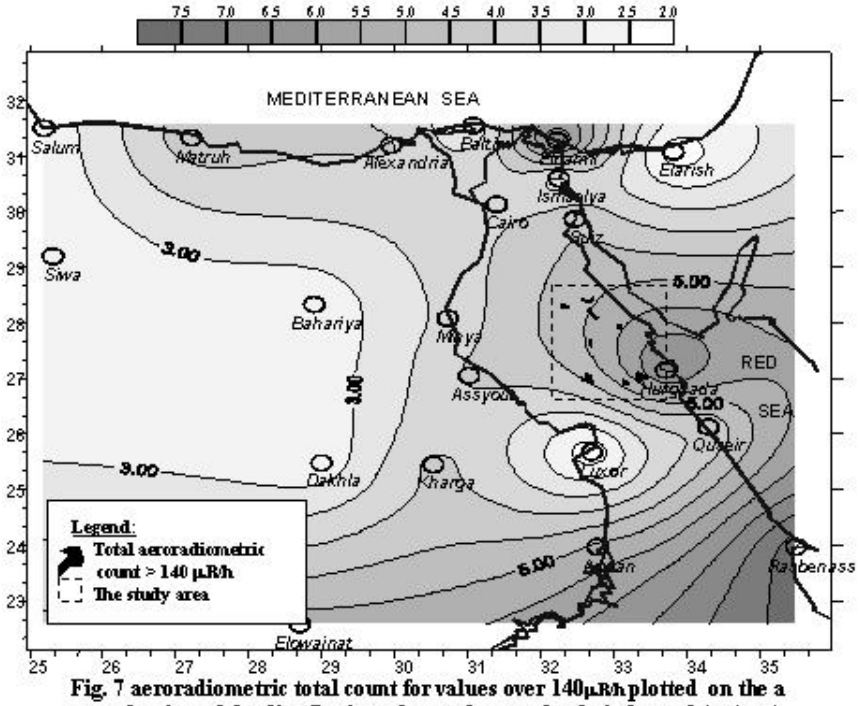

Fig. 7 aeroradiometric total count for values over 140µR/h plotted on the a reproduction of the distribution of annual normals of wind speed (m./sec.) by El-Asrag I.M. et al., (2000),

Geological weathering and erosional processes are responsible for the generation of large amounts of natural dust that enter the hydrosphere and troposphere. Although the process for the generation of natural dust are well understood, little is known of the quantitative studies of natural dust in various remote regions of the globe.

Uranium is a naturally-occurring radioactive substance, very widespread in the earth's crust, but concentrated in certain hard rock formations. As the uranium atoms slowly disintegrate over billions of years, a host of radioactive by-products are formed: thorium-230, radium-226, radon-222 and the infamous "radon daughters," including lead-210 and polonium-210.

As the miners dig the uranium-bearing ore, they inevitably release large quantities of radioactive radon gas into the mine atmosphere. Radon has a relatively short half-life (3.8 days); before long, the air in the mine is heavily contaminated with radon daughters. Adhering to microscopic dust particles, these tiny, pernicious particles are breathed into the miners' and locals' lungs where they lodge delivering a massive dose of alpha radiation to the sensitive lung tissue. The result is an extraordinarily high incidence of lung cancer, fibrosis of the lungs, and other lung diseases, all of which take decades to become manifest.

E- Summary and Conclusion

Through this study, it was able to identify the interpolated density of lineament intersection pattern for selected areas in the region and to check its consistency with their aeroradiometric measurments.The differences in the lineation pattern that is directly affiliated major structural elements in the selected areas and their relation with radiometric variations are distinguished. In this study, the light is shaded on the possiblility of health hazard due to high values of radiometric measurements in study areas.

The DLI analysis is a very powerful technique uses the intersection of the minor fractures associated faults to delineate the main fault directions. The application of this technique on enhanced landsat-5 scenes ratios and 1st principle component of the 7 TM landsat-5 bands give it a unique output by relating the faulting in the area with hydrothermal alteration and iron enrichment along fracture systems or the existing fracturing systems in the study area.

The density of lineaments intersection is counting the number of lineaments intersections per kilometer square. The DLI will help delineate main shear zones. The DLI related to the

enhanced hydrothermaly altered and iron enriched fractures in the area can be observed in figure (2c, 2e, 3c, 3e, 4c, 4e, 5c, and 5e). Since DLI related to the calculated first principle component of the study area which have the largest percentage of the total scene variance, represent the intensity and location of the possible conduits related to most lithologic unit in the area (fig. 2d, 3d, 4d,and 5d).

Concerning the uranium mineralization in the central Eastern Desert, the N-S and NNE-SSW faults and fractures are encountered among the trends associated with uranium mineralization (El Shazly et al., 1979). El Amin (1975) concluded that the uranium bearing hydrothermal solutions rose along major fundamental fractures trending NE-SW and concentrated their uranium mineralization in the N-S and Nne-SSW trending joints. He added that, the association of hematitization and other alteration features with the high δ radioactivity suggests its hydrothermal origin.

Linear patterns distributions in the area around G.Salaat Belih, G. Gattar and G. Abu Harba areas (fig. 5) the NW-SE direction is the most dominant trend in band5/ band 7, band 3/ band 1 as well as aeroradiometric measurements, the NE-SW are strongly recorded at the northern part of G.Gattar.Linear patterns distributions in the area around G. Dara and G. Ghuweirib areas (fig. 2) the NW-SE direction concentrate at the aeroradiometric anomalous zone in band 5/ band 7 and PC1. In contrary the 3/1 show very low values of DLI. Linear patterns distributions in the area around G. Homarat at Esh Mellaha range (fig. 3) the NW-SE direction is restricted along Esh Mellaha in band 5/ band 7, PCA, band 3/ band 1. Linear patterns distributions in the area around G. Um Tweir and G. Abu Marwa, (fig. 4) the high values in PCA and band 3/ band 1 are associated with the NW-SE direction.

References

Abdel Meguid, A. A., 1986. Geologic and radiometric studies of uraniferous granite in Um Ara-Um Shilman area, south Eastern Desert, Egypt. Ph.D. Thesis, Suez Canal University, Egypt.

Amos, B. J., and D. Greenbaum, 1987. Alteration detection using TM imagery: the effects of supergene weathering in an arid environment, in Proceeding of the 21st Symposium on Remote Sensing of Environment: Environmental Research Institute of Michigan, Ann Arbor, Mich., p. 795.

Bennett, S.A., 1993. Use of thematic mapper imagery to identify mineralization in the Santa Teresa district, Sonora, Mexico, Int. Geol. Rev., 35, 1009-1029.

Brickey, D. W., 1986. The use of thematic mapper imagery for mineral exploration in the sedimentary terrain of the Sprine Mountains, Nevada, in Proceeding of the 5th Thematic Conference on Geologic Remote Sensing, Environmental Research Institute of Michigan, Ann Arbor, Mich., pp. 607-613.

Crippen, R. E., 1988a. The dangers of underestimating the importance of data adjustments in band ratioing, Int. J. Remote Sensing, 9, 767-776.

Crippen, R. E., R. G. Blom, and J. R. Heyada, 1988. Directed band ratioing for the retention of perceptually-independent topographic expression in chromaticity-enhanced imagery, Int. J. Remote Sensing, 9, 749-765.

El Amin, H. (1975): Radiometric and geological investigations of El Bakriya area, Eastern Desert, Egypt. Ph.D. Thesis, Cairo Univ., 244p.

El-Asrag, A. M. et al., 2000. Feasibility of clean Energy from wind over Egypt, ICEHM2000,Cairo University, Egypt, September, 2000, page 124-133.

ElFouly, A.A., 2000. Faults and Fractures Intersections Delineation as a Tool for Groundwater Detection Using Remote Sensing and Ground Penetrating Radar Techniques at Saint Catherine area, Southern Sinai, Egypt. ICEHM2000,Cairo University, Egypt, September, 2000, page 293-310.

El Shazly, E. M.; El Kassas, I. A. and Moustafa, E. M. (1979) Comparative fracture analysis and its relation to radioactivity of Um Had pluton, Central Eastern Desert, Egypt. Egypt J. Geol. Vol. 23, No. 1-2, P. 95-110.

Eriksen, A. S., and D. R. Cowan, 1989. Further development and application of GIS technology and geostatistics to assist in the exploration for uranium in western North America, in Proceedings of 7th Thematic Conference on Remote Sensing for Exploration Geology, Vol. II, Environmental Reseach Institute of Michigan, Ann Arbor, Mich., pp. 1285-1307.

Frei, M., and S. L. Jutz, 1989. Use of thematic mapper data for the detection of gold bearing formations in the eastern desert of Egypt, in Proceedings of the 7th Thematic Conference on Remote Sensing for Exploration Geology, Vol. II, Environmental Research Institute of Michigan, Ann Arbor, Mich., pp. 1157-1172.

Geological Survey of Egypt, 1994. Geologic Map of Sinai- Sheet NO1.

Hutsinpiller, A., 1988. Discrimination of hydrothermal alteration mineral assemblages at Virginia City, Nevada, using the airborne imaging spectrometer, Remote Sensing Environ., 24, 53-66.

Kowalczyk, P., and K. Logan, 1989. TM processing for routine use in mineral exploration, in Proceedings of the 7th Thematic Conference on Remote Sensing for Exploration Geology, Vol. I, Environmental Research Institute of Michigan, Ann Arbor, Mich., pp. 323-329.

Mouat, D. A., J.S. Myers, and N. M. Miltron, 1986, An Integrated approach to the use of landsat TM data for gold exploration in west-central Nevada, in Proceedings of the 5th Thematic Conference on Geologic Remote Sensing, Environmental Research Institute of Michigan, Ann Arbor, Mich., pp. 431-443.

Rodriguez, E. P., and C. E. Glass, 1991. Digital analysis for mineral exploration at the Puerto Libertad area, Sonora, Mexico, in Proceedings of the 8th Thematic Conference on Geologic Remote Sensing, Vol. II, Environmental Research Institute of Michigan, Ann Arbor, Mich., pp. 851-862.

Sabins, F.F., and R. M., Miller, 1994. Resource assessment: Salar de Uyuni and Vicinity, Bolovia, in Proceedings of the 10th Thematic Conference on Geologic Remote Sensing, Vol. I, Environmental Research Institute of Michigan, Ann Arbor, Mich., pp. 92-103.

Wilcox, R. E., Harding, T. P., and Seely, D. R., 1973, Basic wrench tectonics: American Association of Petroleum Geologists Bulletin, v. 57. 74-96.